CONSIDERATION OF POD INTERPOLATION FOR AEROELASTIC DESIGN WITH LARGE GLOBAL STRUCTURAL VARIATIONS USE STRUCTURAL DYNAMIC REANALYSIS

Dongfeng Li[1,2], Gang Chen[1,2*], A.Da Ronch[3], Qiang Zhou[1,2], Yueming Li[1,2]

[1] State Key Laboratory for Strength and Vibration of Mechanical Structures, School of Aerospace, Xi'an Jiaotong University, Xi'an, 710049, China
aachengang@xjtu.edu.cn

[2] Shannxi Key Laboratory for Environment and Control of Flight Vehicle, Xi'an Jiaotong University, Xi'an, 710049, China

[3] Faculty of Engineering and the Environment, University of Southampton, Southampton SO17 1BJ, UK
A.Da-Ronch@soton.ac.uk

Keywords:reduced order model, proper orthogonal decomposition, transonic aeroelasticity, flutter boundary, structural dynamic reanalysis.

Abstract: An efficient approximate POD/ROM reconstruction method was proposed that can use the existing CFD-based POD/ROMs to rapidly obtain the new aeroelastic responses when structural parameters of the transonic aeroelastic system are changed at global level. The approximate method is illustrated and verified by the AGARD 445.6 wing model with different structural parameter variation. The simulation results show that proposed new POD/ROM reconstruction method can accurately capture the new aeroelastic responses and flutter boundary corresponding to the changed system with high efficiency. The proposed method extend the traditional POD/ROM from fix structural aeroelastic system to those with large global structural variations.

1 INTRODUCTION

To obviate the costs involved in solving complex fluid models of large size, researchers have developed CFD-based unsteady aerodynamic reduced order models (ROMs)[1-4]. These models extract key data of the fluid systems to generate a low dimensional system that retains similar accuracy of the full order model while reducing significantly the costs. System identification and proper orthogonal decomposition (POD) are among the most popular ROMs for nonlinear aeroelastic analysis. For example, Dowell [5] and Lucia [6] demonstrated the use of ROMs to investigate transonic limit-cycle oscillation (LCO). Raveh [7] reported on ROMs for gust load analysis in the transonic regime, investigating both discrete and continuous gust responses. The POD method, in particular, has been successfully applied to the aeroelastic analysis of turbine blades [8, 9]，helicopter rotor blade [10], wings [11-13] and complete aircraft configurations [14, 15]. More recently, the POD has been exercised for transonic aeroelastic analysis [16], active aeroelastic control [17], LCO control [18], gust response analysis [19], and transonic flutter suppression with control delay [20].

The largest efforts in the ROM community are addressed at improving the model predictions at a fixed flight condition for a frozen aeroelastic model configuration. Changes to either flight conditions (Mach number, angle of attack, etc.) or model configuration (mass,

geometry, etc.) are neglected for the difficulty of accounting these effects within a single ROM. The limited body of work on this topic consists of the following publications available in the open literature. Epureanu [21] and Lieu [22-24] used ROMs to predict the transonic aeroelastic response with variations of the free stream Mach number and angle of attack. Chen [25] proposed a nonlinear POD technique, Chen [26] discussed a support-vector-machine based ROM, and Chen [27] presented a linear parameter-varying (LPV) valid for bounded changes of the flow conditions. Even fewer studies have shown the ability to capture changes in the mass and stiffness distribution of an aircraft structure within a single aeroelastic ROM. As the aircraft design process progresses through maturity gates, with the outer shape being frozen at the early stages, the structural model undergoes multiple changes to guarantee the design target loads are met. Structural modeshapes and associated frequencies are dependent upon the mass and stiffness distribution, and this should be carefully included in an aeroelastic analysis, Hayes [28]. When a structural modification is made, the structural model should be updated and the new modeshapes and frequencies recalculated. In an aeroelastic analysis, the influence of changes in the structural model will also propagate to the fluid solution, with both mean and unsteady flow components dependent upon the structural model. One approach to update the aeroelastic ROM, referred to as the direct approach, is the regeneration of the model. For every change of the structural model, this entails calculating: a) the new set of modeshapes and frequencies; b) the mean flow solution that guarantees the aeroelastic equilibrium; and c) the ROM around the new equilibrium position[29-32].

Rather than reconstructing a new POD/ROMs as the direct method, the innovation of the paper is that we proposed an new approximate aeroelastic ROM interpolation method by introducing the approximate structural dynamic reanalysis method with structural parameters modification to the traditional ROM construction procedure. It is means that we proposed an approximate dynamic reanalysis based ROM Interpolation method, thus an new structural parameterization POD/ROM, which would be expect to have the great potential to extend the application of the traditional aeroelastic ROM to aeroelastic optimization and uncertainty analysis in transonic flow. The paper is constructed as follows: Sec.2 give the brief introduction of the standard POD/ROM construction procedure for aeroelastic systems; Sec.3 give a description on the approximate dynamic reanalysis based aeroelastic analysis method firstly, and then introduce the proposed incorporation procedure of the structural reanalysis algorithm with the POD/ROM construction method for the aeroelastic models with global structural parameter variation; In Sec.4 the proposed new ROM interpolation method was demonstrated and evaluated by the AGARD 445.6 aeroelastic wing model with global level structural parameters variation in transonic flow. Sec. 5 is the conclusion and discussion of the proposed method.

2 CFD-BASED REDUCED ORDER MODEL FOR AEROELASTIC SYSTEM

2.1 Flow and Structural Solver

A nonlinear aeroelastic system can be represented by the two-field arbitrary Lagrangian-Eulerian (ALE) method, in which the governing equation of the nonlinear aeroelastic system can be written as

$$\frac{d(\mathbf{A}\cdot\mathbf{w})}{dt}+\mathbf{F}(\mathbf{w})=\mathbf{0} \tag{1}$$

$$\mathbf{M}\ddot{\mathbf{d}}+\mathbf{D}\dot{\mathbf{d}}+\mathbf{K}\mathbf{d}=\mathbf{f} \tag{2}$$

Eq. (1) represents a finite volume discretization of the ALE non-dimensional conservative form of the Navier–Stokes equations. Here, **A** is a diagonal matrix containing the cell volumes, **F** is the nonlinear numerical flux function, **w** is the conservative state vector of the fluid subsystem, and **d** is the vector of structure displacements. Eq. (2) is for a finite element discretization of the structural dynamic equations. **M**, **D**, and **K** are the mass, damping, and stiffness matrices, respectively. **f** is the vector of aerodynamic loads at the structural grid points, derived from solving Eq. (1).

2.2 CFD/CSD coupling simulation

The CFD solver employs Cartesian grids, using a multi-block structured cell-centered finite volume discretisation, and the second-order Van Leer scheme [33] is used for the spatial discretization. The dual time-stepping [34] and Lower-Upper Symmetric Gauss-Seidel (LU-SGS) implicit method [35] are used for time integration. A modal representation of the structural model is used. Using generalized (or modal) coordinates **u**, the structural displacement field may be expressed in the form $\mathbf{d} = \mathbf{\Phi u}$, where $\mathbf{\Phi} = [\boldsymbol{\phi}^1, \boldsymbol{\phi}^2, ...]$ denotes the modal matrix. It follows that Eq. (2) may be rewritten as:

$$\bar{\mathbf{M}} \cdot \ddot{\mathbf{u}} + \bar{\mathbf{D}} \cdot \dot{\mathbf{u}} + \bar{\mathbf{K}} \cdot \mathbf{u} = \mathbf{f}_{gen} \tag{3}$$

where $\bar{\mathbf{M}} = \mathbf{\Phi}^T \mathbf{M} \mathbf{\Phi}$, $\bar{\mathbf{D}} = \mathbf{\Phi}^T \mathbf{D} \mathbf{\Phi}$ and $\bar{\mathbf{K}} = \mathbf{\Phi}^T \mathbf{K} \mathbf{\Phi}$ are the generalized mass, damping and stiffness matrices, respectively. $\mathbf{f}_{gen}$ is the vector of generalized aerodynamic forces:

$$\mathbf{f}_{gen} = \mathbf{\Phi}^T \mathbf{f} \text{ or for vector element } i\text{: } \mathbf{f}_{gen}^i = q_\infty \cdot \int_{\mathbf{s}} c_p \cdot \boldsymbol{\phi}^i \circ d\mathbf{S} \tag{4}$$

where $\mathbf{f}_{gen}^i$ is i-th generalized aerodynamic forces, q_∞ is the free stream dynamic pressure, c_p is pressure coefficient.

A time-domain, fully-implicit, loosely-coupled partitioned approach is employed for the unsteady fluid-structure interaction (FSI) analysis. The process is illustrated in **Fig. 1**. A converged steady-state flow solution is used to initiate the FSI iteration loop. The transfer of the aerodynamic loads from the fluid to the structural field, and the transfer of the structural displacements from the structural to the aerodynamic field are performed using the infinite plate spline (IPS) method [36]. The radial basis functions (RBFs), combined with the transfinite interpolation (TFI) algorithm [37], are then used to warp the fluid volume mesh, based on the new deformed surface grid obtained by mapping the structural displacements to the fluid surface grid. The iterative process continues until the change in the structural displacements is below a given threshold, or the maximum number of iterations is reached. The coupled aeroelastic solver has been exercised on several two and three-dimensional aeroelastic models. The reader may find more details in [16, 20, 38].

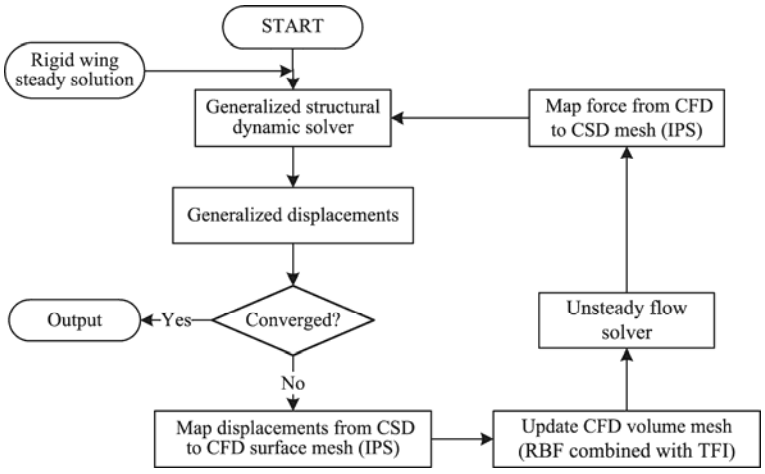

Figure 1: Flow chart of the fluid-structure coupling algorithm

2.3 POD/ROM Method for Aeroelastic Modeling

The POD method finds common use in providing a compact description of large computational models as, for example, in approximating the spatial and temporal characteristics of unsteady transonic flows for aeroelastic analysis [39, 40]. First, the unsteady flow equations are linearized around a mean flow solution (equilibrium). The linearized flow solver is then used to obtain the POD snapshots for the generation of the unsteady aerodynamic ROM. Denoting ($\Delta\mathbf{w}, \Delta\mathbf{u}, \Delta\dot{\mathbf{u}}$)small perturbation around the equilibrium ($\mathbf{w}_0, \mathbf{u}_0, \dot{\mathbf{u}}_0$),one obtains the linearized flow equations:

$$\mathbf{A}_0\dot{\mathbf{w}} + \mathbf{H}\mathbf{w} + (\mathbf{E}+\mathbf{C})\dot{\mathbf{u}} + \mathbf{G}\mathbf{u} = \mathbf{0} \tag{5}$$

where

$$\mathbf{H} = \frac{\partial \mathbf{F}}{\partial \mathbf{w}}(\mathbf{w}_0, \mathbf{u}_0, \dot{\mathbf{u}}_0) \qquad \mathbf{G} = \frac{\partial \mathbf{F}}{\partial \mathbf{u}}(\mathbf{w}_0, \mathbf{u}_0, \dot{\mathbf{u}}_0)$$
$$\mathbf{E} = \frac{\partial \mathbf{A}}{\partial \mathbf{u}}\mathbf{w}_0 \qquad \mathbf{C} = \frac{\partial \mathbf{F}}{\partial \dot{\mathbf{u}}}(\mathbf{w}_0, \mathbf{u}_0, \dot{\mathbf{u}}_0)$$

The matrix **H** is the gradient of the numerical flux function with respect to the vector of fluid variables. Matrices **G** and **C** are the gradients of the flux function with respect to the generalized coordinates and their velocities, respectively. Finally, the matrix **E** indicates the gradient of the cell volumes with respect to the generalized coordinates. Note that the matrices **G**, **E** and **C** need to be recomputed if the structural parameters are changed.

The linearization of the structural dynamic equation around an equilibrium state can be written as follows:

$$\bar{\mathbf{M}}\ddot{\mathbf{u}} + \bar{\mathbf{D}}_0\dot{\mathbf{u}} + \bar{\mathbf{K}}_s\mathbf{u} = \mathbf{P}_0\mathbf{w} \tag{6}$$

where

$$\bar{\mathbf{K}}_0 = \frac{\partial \mathbf{f}^{int}}{\partial \mathbf{u}}(\mathbf{u}_0, \dot{\mathbf{u}}_0) \qquad \bar{\mathbf{K}}_s = \bar{\mathbf{K}}_0 - \frac{\partial \mathbf{f}^{ext}}{\partial \mathbf{u}}(\mathbf{w}_0, \mathbf{u}_0)$$
$$\bar{\mathbf{D}}_0 = \frac{\partial \mathbf{f}^{int}}{\partial \dot{\mathbf{u}}}(\mathbf{u}_0, \dot{\mathbf{u}}_0) \qquad \mathbf{P}_0 = \frac{\partial \mathbf{f}^{ext}}{\partial \mathbf{w}}(\mathbf{w}_0, \mathbf{u}_0)$$

For the analysis of the system stability, the terms $\frac{\partial \mathbf{f}^{ext}}{\partial \mathbf{u}}$ and $\bar{\mathbf{D}}_0$ can be neglected [23], which leads to the structural dynamic equation such as:

$$\bar{\mathbf{M}}\ddot{\mathbf{u}} + \bar{\mathbf{K}}_0\mathbf{u} = \mathbf{P}_0\mathbf{w} \tag{7}$$

The aeroelastic stability is studied as an eigenvalue problem [41]. Using the linearized flow and structural equations derived in Eqs. (5) and (7), the generalized eigenvalue problem is:

$$(\mathbf{N} - \zeta_i\boldsymbol{\Theta})\mathbf{q}_i = \mathbf{0} \tag{8}$$

where ζ_i indicates the *i*-th eigenvalue and $\mathbf{q}_i$ the corresponding eigenvector, and

$$\mathbf{N} = \begin{bmatrix} \mathbf{H} & (\mathbf{E}+\mathbf{C}) & \mathbf{G} \\ -\mathbf{P} & \mathbf{0} & \mathbf{K}_0 \\ \mathbf{0} & \mathbf{I} & \mathbf{0} \end{bmatrix},\ \boldsymbol{\Theta} = \begin{bmatrix} \mathbf{A} & \mathbf{0} & \mathbf{0} \\ \mathbf{0} & \mathbf{M} & \mathbf{0} \\ \mathbf{0} & \mathbf{0} & \mathbf{I} \end{bmatrix},\ \mathbf{q} = \begin{bmatrix} \mathbf{w} \\ \dot{\mathbf{u}} \\ \mathbf{u} \end{bmatrix}.$$

A ROM of the unsteady flow is considered in this work, based on the POD technique. The POD method aims at reconstructing the behavior of the overall system using an orthogonal basis set with much smaller number of degrees of freedom. Denote $\{\mathbf{x}^k\}$, $k = 1,2,3\ldots m$, a set of data, with $\mathbf{x}^k$ is the *n*-dimensional space, and *m* is the number of snapshots. The POD method searches an *m*-dimensional proper orthogonal subspace, $\boldsymbol{\Psi} \in \mathbf{R}^{n\times m}$, to minimize the mapping errors from $\boldsymbol{\Psi}$

$$\mathbf{G} = \min_{\boldsymbol{\Phi}} \sum_{k=1}^{m} \left\| \mathbf{x}^k - \boldsymbol{\Omega}\boldsymbol{\Omega}^T\mathbf{x}^k \right\| = \sum_{k=1}^{m} \left\| \mathbf{x}^k - \boldsymbol{\Psi}\boldsymbol{\Psi}^T\mathbf{x}^k \right\|,\ \boldsymbol{\Omega}^H\boldsymbol{\Omega} = \mathbf{I} \tag{9}$$

The minimization problem is equivalent to

$$\mathbf{H} = \max_{\boldsymbol{\Phi}} \sum_{k=1}^{m} \frac{\left\langle \left(\mathbf{x}^k, \boldsymbol{\Omega}\right)^2 \right\rangle}{\|\boldsymbol{\Omega}\|^2} = \sum_{k=1}^{m} \frac{\left\langle \left(\mathbf{x}^k, \boldsymbol{\Psi}\right)^2 \right\rangle}{\|\boldsymbol{\Psi}\|^2},\ \boldsymbol{\Omega}^H\boldsymbol{\Omega} = \mathbf{I} \tag{10}$$

The constraint optimization problem in Eq. (6) is transformed into the following Lagrange equation

$$J(\boldsymbol{\Omega}) = \sum_{k=1}^{m} \left(\mathbf{x}^k, \boldsymbol{\Omega}\right)^2 - \lambda\left(\|\boldsymbol{\Omega}\|^2 - 1\right) \tag{11}$$

Solving the partial derivative of the objective function $J(\boldsymbol{\Phi})$ with respect to $\boldsymbol{\Phi}$ gives

$$\frac{d}{d\boldsymbol{\Omega}} J(\boldsymbol{\Omega}) = 2\mathbf{X}\mathbf{X}^H\boldsymbol{\Omega} - 2\lambda\boldsymbol{\Omega} \tag{12}$$

where $\mathbf{X} = \{\mathbf{x}_1, \mathbf{x}_2, \cdots \mathbf{x}_m\} \in \mathbf{R}^{n\times m}$ is a matrix containing *m* snapshots as columns. By setting Eq. (12) to zero; thus, the following equation is obtained:

$$\left(\mathbf{X}\mathbf{X}^T - \xi\mathbf{I}\right)\boldsymbol{\Psi} = 0 \tag{13}$$

The problem is transformed into solving the eigenvalue problem of the POD kernel, $\mathbf{X}\mathbf{X}^H$. The eigenvalue problem has very large size, as $\mathbf{X}\mathbf{X}^H \in \mathbf{R}^{n\times n}$. Because $\mathbf{X}\mathbf{X}^H$ and $\mathbf{X}\mathbf{X}^H$ have the same eigenvalues, so we can obtain $\boldsymbol{\Psi}$ as following equation [41]:

$$\begin{cases} \mathbf{X}\mathbf{X}^T\mathbf{V} = \mathbf{V}\boldsymbol{\Lambda} \\ \boldsymbol{\Psi} = \mathbf{X}\mathbf{V}\boldsymbol{\Lambda}^{-1/2} \end{cases} \tag{14}$$

where $\boldsymbol{\Psi} = [\boldsymbol{\psi}_1, \boldsymbol{\psi}_2, \ldots, \boldsymbol{\psi}_m]$, $\boldsymbol{\Lambda} = diag(\xi_1, \xi_2 \cdots \xi_m)$, $\xi_1 \geq \xi_2 \geq, \ldots, \geq \xi_m$. The value of ξ_i represents the contribution of the *i*-th snapshot to the original system. To build an aeroelastic ROM, it is typically possible to retain the first *r*-order POD modes $\boldsymbol{\Psi}_r = [\boldsymbol{\psi}_1, \boldsymbol{\psi}_2, \ldots, \boldsymbol{\psi}_r]$ while retaining most of the energy of the original system. By projecting the full-order series $\mathbf{x}^{n\times 1}$ on the *r*-order POD modes $\boldsymbol{\Psi}_r = [\boldsymbol{\psi}_1, \boldsymbol{\psi}_2, \ldots, \boldsymbol{\psi}_r]$, we can reduced the full order system to a reduced *r*-order system

$$\begin{cases} \dot{\mathbf{x}}_r = \boldsymbol{\Psi}_r^T \mathbf{A} \boldsymbol{\Psi}_r \mathbf{x}_r + \boldsymbol{\Psi}_r^T \mathbf{B} \mathbf{y} \\ \mathbf{f}^{ext} = \mathbf{C} \boldsymbol{\Psi}_r \mathbf{x}_r \end{cases} \tag{15}$$

where $\mathbf{A} = -\mathbf{A}_0^{-1}\mathbf{H}$, $\mathbf{B} = -\mathbf{A}_0^{-1}\left[\mathbf{E} + \mathbf{C}\ \mathbf{G}\right]$, $\mathbf{y} = \left[\dot{\mathbf{u}}\ \mathbf{u}\right]^T$, $\mathbf{C} = \mathbf{P}$. Here, $\mathbf{A}$, $\mathbf{B}$, and $\mathbf{y}$ can be considered as the system inputs, and the $\mathbf{f}^{ext}$ is the system output.

In summary, above POD process outlined can be used for constructing a fluid ROM for prescribed modeshapes. The corresponding aeroelastic responses is obtained by coupling Eq. (7) with Eq. (15).

3 ROM INTERPOLATION METHOD BASED APPROXIMATE DYNAMIC REANALYSIS

3.1 Approximate structural dynamic reanalysis method

In the optimization of structural systems, it is very important to re-compute the eigenvalues of the structures when the parameters of the structures are changed. In many cases, one of main obstacles is the high computational cost involved in the solution of a large-scale eigenvalue problem. To this goal, a number of methods have been proposed to ease the eigenvalue reanalysis for the modified structures. Generally, methods are classified into two categories [42]. First, direct methods are commonly based on the Sherman-Morrison-Woodbury (SMW) formula [43] that is applicable for large but local (or low-rank) modifications. The drawback of these methods is that they are limited by the scale of the problem or rank of the modification, and are not suitable for global modifications of the structural parameters. Direct methods also suffer from high computational costs. As an alternative to direct methods, approximate methods [44-46] aim at obtaining the frequencies and modeshapes for the modified structures without resolving the eigenproblem. The advantage in doing so is a significant reduction of the computational costs, and the applicability is extended for global (or high-rank) modifications of the structures. The extended Kirsch combined method [45, 47] is an efficient approach for the case of large modifications of the structural parameters. More details relevant to this work are given next.

For the structural dynamic equations Eq. (3), consider a structure with stiffness matrix $\mathbf{K}_0$ and mass matrix $\mathbf{M}_0$. The corresponding frequencies λ_0^i and modeshapes $\boldsymbol{\Phi}_0 = [\boldsymbol{\phi}_0^1, \boldsymbol{\phi}_0^2, ...]$ are calculated by solving the generalized eigenproblem:

$$\mathbf{K}_0 \boldsymbol{\phi}_0^i = \lambda_0^i \mathbf{M}_0 \boldsymbol{\phi}_0^i \tag{16}$$

which will be referred to as the original problem (indicated by the subscript 0). When the structural parameters are changed, the stiffness and mass matrices are perturbed into the form $\mathbf{K}_0 + \Delta\mathbf{K}$ and $\mathbf{M}_0 + \Delta\mathbf{M}$, respectively. The terms $\Delta\mathbf{K}$ and $\Delta\mathbf{M}$ denote the perturbations in the stiffness and mass matrix, respectively. The eigenvalue problem for modified structural parameters becomes:

$$\mathbf{K} \boldsymbol{\phi}^i = \lambda^i \mathbf{M} \boldsymbol{\phi}^i \tag{17}$$

where λ^i is i-th eigenvalue of the modified structure, $\boldsymbol{\phi}^i$ is i-th eigenvector of the modified structure.

The extended Kirsch combined method use the second-order eigenvector terms [48] as the basis vectors in the following modeshapes reduced basis:

$$\boldsymbol{\phi}^i = \boldsymbol{\phi}_B^i \mathbf{z}^i \tag{18}$$

where

$$\boldsymbol{\phi}_B^i = \left[\boldsymbol{\phi}_0^i,\ \boldsymbol{\phi}_1^i,\ \boldsymbol{\phi}_2^i\right] \tag{19}$$

$$\mathbf{z}^i = (z_0^i,\ z_1^i,\ z_2^i)^T \in \mathbf{R}^{3\times 1} \tag{20}$$

$$\boldsymbol{\phi}_1^i = \sum_{s=1,s\neq i}^{n} \frac{1}{\lambda_0^i - \lambda_0^s}[(\boldsymbol{\phi}_0^s)^T(\Delta\mathbf{K} - \lambda_0^i\Delta\mathbf{M})\boldsymbol{\phi}_0^i]\boldsymbol{\phi}_0^s - \frac{1}{2}[(\boldsymbol{\phi}_0^i)^T\Delta\mathbf{M}\boldsymbol{\phi}_0^i]\boldsymbol{\phi}_0^i = \boldsymbol{\phi}_0\mathbf{Z}_1^i \tag{21}$$

$$\begin{aligned}\boldsymbol{\phi}_2^i = &\sum_{s=1,s\neq i}^{n} \frac{1}{\lambda_0^i - \lambda_0^s}[(\boldsymbol{\phi}_0^s)^T(\Delta\mathbf{K} - \lambda_0^i\Delta\mathbf{M})\boldsymbol{\phi}_1^i - \lambda_1^i(\boldsymbol{\phi}_0^s)^T(\mathbf{M}_0\boldsymbol{\phi}_1^i + \Delta\mathbf{M}\boldsymbol{\phi}_0^i)]\boldsymbol{\phi}_0^s \\ &-\frac{1}{2}[(\boldsymbol{\phi}_0^i)^T\Delta\mathbf{M}\boldsymbol{\phi}_1^i + (\boldsymbol{\phi}_1^i)^T(\mathbf{M}_0\boldsymbol{\phi}_1^i + \Delta\mathbf{M}\boldsymbol{\phi}_0^i)]\boldsymbol{\phi}_0^i = \boldsymbol{\phi}_0\mathbf{Z}_2^i\end{aligned} \tag{22}$$

where $\boldsymbol{\phi}_1^i$ and $\boldsymbol{\phi}_2^i$ are the *i*-th first-order and second-order eigenvector of the modified structure, respectively. The coefficient vector, $\mathbf{z}^i$, contains three unknowns (for a second-order perturbation). Substituting Eq. (21) and Eq. (22) into Eq. (18), $\boldsymbol{\Phi}$ can be written as

$$\boldsymbol{\Phi} = \begin{bmatrix} \boldsymbol{\phi}_0^1 \ldots \boldsymbol{\phi}_0^i & \mathbf{0} & \mathbf{0} \\ \mathbf{0} & \boldsymbol{\phi}_0^1 \ldots \boldsymbol{\phi}_0^i & \mathbf{0} \\ \mathbf{0} & \mathbf{0} & \boldsymbol{\phi}_0^1 \ldots \boldsymbol{\phi}_0^i \end{bmatrix} \begin{bmatrix} \mathbf{I}_0^1 \ldots \mathbf{I}_0^i & \mathbf{0} & \mathbf{0} \\ \mathbf{0} & \mathbf{Z}_1^1 \ldots \mathbf{Z}_1^i & \mathbf{0} \\ \mathbf{0} & \mathbf{0} & \mathbf{Z}_2^1 \ldots \mathbf{Z}_2^i \end{bmatrix}^T \begin{bmatrix} \mathbf{z}^1 & \mathbf{0} & \mathbf{0} \\ \mathbf{0} & \mathbf{z}^2 & \mathbf{0} \\ \mathbf{0} & \mathbf{0} & \mathbf{z}^3 \end{bmatrix} = \boldsymbol{\Phi}_0\mathbf{Z} \tag{23}$$

where

$$\mathbf{Z} = \begin{bmatrix} \mathbf{I}_0^1 \ldots \mathbf{I}_0^i & \mathbf{0} & \mathbf{0} \\ \mathbf{0} & \mathbf{Z}_1^1 \ldots \mathbf{Z}_1^i & \mathbf{0} \\ \mathbf{0} & \mathbf{0} & \mathbf{Z}_2^1 \ldots \mathbf{Z}_2^i \end{bmatrix}^T \begin{bmatrix} \mathbf{z}^1 & \mathbf{0} & \mathbf{0} \\ \mathbf{0} & \mathbf{z}^2 & \mathbf{0} \\ \mathbf{0} & \mathbf{0} & \mathbf{z}^3 \end{bmatrix} \tag{24}$$

Substituting Eq. (18) into the modified analysis equations Eq. (17), and premultiplying by $(\boldsymbol{\phi}_B^i)^T$, one obtains:

$$(\boldsymbol{\phi}_B^i)^T(\mathbf{K}_0 + \Delta\mathbf{K})\boldsymbol{\phi}_B^i\mathbf{z}^i = \lambda^i(\boldsymbol{\phi}_B^i)^T(\mathbf{M}_0 + \Delta\mathbf{M})\boldsymbol{\phi}_B^i\mathbf{z}^i \tag{25}$$

Introducing the notation

$$\mathbf{K}_R^i = (\boldsymbol{\phi}_B^i)^T(\mathbf{K}_0 + \Delta\mathbf{K})\boldsymbol{\phi}_B^i \tag{26}$$

$$\mathbf{M}_R^i = (\boldsymbol{\phi}_B^i)^T(\mathbf{M}_0 + \Delta\mathbf{M})\boldsymbol{\phi}_B^i \tag{27}$$

and substituting Eq. (26) and (27) into Eq. (18), we can obtain a set of (3×3) matrix equation

$$\mathbf{K}_R^i\mathbf{z}^i = \lambda^i\mathbf{M}_R^i\mathbf{z}^i \tag{28}$$

Thus, the coefficient vector $\mathbf{z}^i$ is evaluated from Eq. (28). The *i*-th eigenvector of the modified structure is obtained by substituting $\mathbf{z}^i$ into Eq. (18) and $\mathbf{Z}$ is obtained by substituting $\mathbf{z}^i$ into Eq. (24).

Finally, the *i*-th eigenvalue of the modified structure, λ_K^i, is computed using Rayleigh quotient:

$$\lambda_K^i = \frac{(\boldsymbol{\phi}^i)^T(\mathbf{K}_0 + \Delta\mathbf{K})\boldsymbol{\phi}^i}{(\boldsymbol{\phi}^i)^T(\mathbf{M}_0 + \Delta\mathbf{M})\boldsymbol{\phi}^i} \tag{29}$$

To summarize, the extended Kirsch combined method involves the following operations:

(1) Solve the eigenvalue problem for the original structure, Eq. (16), and calculate the mass and stiffness matrices of the modified structure, $\mathbf{K}_0 + \Delta\mathbf{K}$ and $\mathbf{M}_0 + \Delta\mathbf{M}$, respectively;
(2) Compute first and second-order perturbations of the eigenvector of the modified structure, Eqs. (21) and (22);
(3) Form the stiffness and mass matrices ($\mathbf{K}_R^i$ and $\mathbf{M}_R^i$) of the reduced system corresponding to the *i*-th eigenvector using Eq. (26) and Eq. (27);
(4) Use Eq. (28) to calculate the coefficients $\mathbf{z}^i$;
(5) Substitute **z** into Eq. (24) to get a constant matrix **Z** and use Eq. (18) to compute the approximate eigenvectors $\boldsymbol{\Phi}$;
(6) Finally, compute the approximate eigenvalue λ_K^i using Rayleigh quotient by Eq. (29).

3.2 Reanalysis algorithm based POD/ROM interpolation method

The modeshapes $\boldsymbol{\Phi}_0$ of the original structure is taken as the basic modeshapes for basic POD/ROM construction. For modified structure, the physical displacement of the wing can be written as

$$\mathbf{d} = \boldsymbol{\Phi}\mathbf{u} \tag{30}$$

Substituting Eq. (23) into Eq. (30), the physical displacement of the wing can also be written as

$$\mathbf{d} = \boldsymbol{\Phi}_0(\mathbf{Z}\mathbf{u}) \tag{31}$$

and $\mathbf{u}_b = \mathbf{Z}\mathbf{u}$, $\mathbf{u}_b$ is artificially defined as basic generalized displacements.

A change of the structural parameters affects the matrices **H**, **G**, **E** and **C** of the linearized flow solver, Eq. (9). Substituting the relation $\mathbf{u}_b = \mathbf{Z}\mathbf{u}$, the matrices may be rewritten in terms of the vector of basic generalized displacements:

$$\mathbf{G} = \frac{\partial\mathbf{F}}{\partial\mathbf{u}}(\mathbf{w}_0, \mathbf{u}_0, \dot{\mathbf{u}}_0) = \frac{\partial\mathbf{F}}{\mathbf{Z}^{-1}\partial\mathbf{u}_b}(\mathbf{w}_0, \mathbf{u}_0, \dot{\mathbf{u}}_0) = \mathbf{Z}\mathbf{G}_b$$

$$\mathbf{E} = \frac{\partial\mathbf{A}}{\partial\mathbf{u}}\mathbf{w}_0 = \frac{\partial\mathbf{A}}{\mathbf{Z}^{-1}\partial\mathbf{u}_b}\mathbf{w}_0 = \mathbf{Z}\mathbf{E}_b$$

$$\mathbf{C} = \frac{\partial\mathbf{F}}{\partial\dot{\mathbf{u}}}(\mathbf{w}_0, \mathbf{u}_0, \dot{\mathbf{u}}_0) = \frac{\partial\mathbf{F}}{\mathbf{Z}^{-1}\partial\dot{\mathbf{u}}_b}(\mathbf{w}_0, \mathbf{u}_0, \dot{\mathbf{u}}_0) = \mathbf{Z}\mathbf{C}_b$$

where $\mathbf{G}_b$, $\mathbf{E}_b$, $\mathbf{C}_b$ are the first order terms in a Taylor series expansion of the basis reduced *r*-order system aeroelastic. Now, the reduced fluid model of modified structure is written as

$$\begin{cases} \dot{\mathbf{x}}_r = \boldsymbol{\Psi}_r^T\mathbf{A}\boldsymbol{\Psi}_r\mathbf{x}_r + \boldsymbol{\Psi}_r^T\mathbf{Z}\mathbf{B}_b\mathbf{y} \\ \mathbf{f}^{ext} = \mathbf{Z}\mathbf{C}_b\boldsymbol{\Psi}_r\mathbf{x}_r \end{cases} \tag{32}$$

where $\mathbf{A} = -\mathbf{A}_0^{-1}\mathbf{H}$, $\mathbf{B}_b = -\mathbf{A}_0^{-1}\left[\mathbf{E}_b + \mathbf{C}_b \;\; \mathbf{G}_b\right]$, $\mathbf{y} = \left[\dot{\mathbf{u}} \;\; \mathbf{u}\right]^T$, $\mathbf{C}_b = \mathbf{P}_b$.

The structural dynamic equations of modified structure are:

$$\bar{\mathbf{M}}\ddot{\mathbf{u}} + \bar{\mathbf{K}}\mathbf{u} = \mathbf{f}^{ext} \tag{33}$$

here, $\bar{\mathbf{M}} = \mathbf{Z}^T\boldsymbol{\Phi}_0^T(\mathbf{M}+\Delta\mathbf{M})\boldsymbol{\Phi}_0\mathbf{Z}$, $\bar{\mathbf{K}} = \mathbf{Z}^T\boldsymbol{\Phi}_0^T(\mathbf{K}+\Delta\mathbf{K})\boldsymbol{\Phi}_0\mathbf{Z}$. In addition, when $\Delta\mathbf{K}=\mathbf{0}$, $\Delta\mathbf{M}=\mathbf{0}$, $\mathbf{Z}$ is the unit matrix, Eq. (32) and Eq. (33) are equivalent to Eq. (15) and Eq. (7), respectively.

The vector of generalized aerodynamic loads $\mathbf{f}^{ext}$ corresponding to the new modeshapes $\boldsymbol{\Phi}$ of the global modification structural model can ben rapidly calculated without the expensive time-consuming reconstruction procedure of the new POD basis.

The proposed appropriate structural dynamic reanalysis based POD/ROM interpolation method is illustrated in **Fig. 2**.

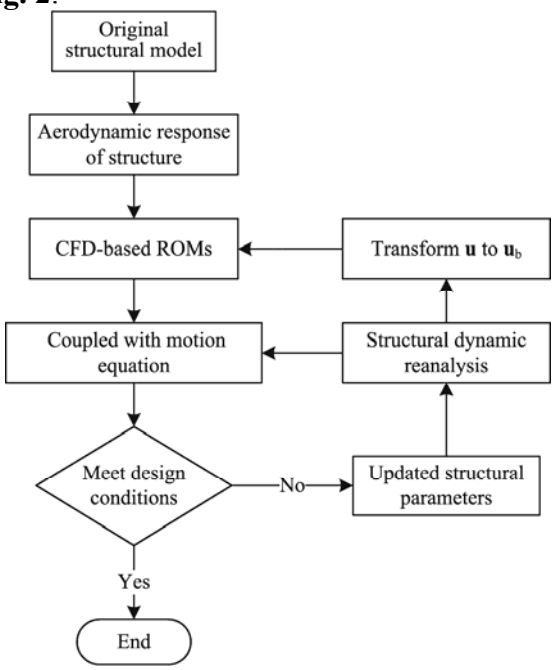

Figure 2 Flow chart of approximate method

Per Fig. 2, the proposed POD/ROM interpolation algorithm is summarized as followings:

(1) Establish CFD-based POD/ROMs based on the basis modeshapes;
(2) Use Extended Kirsch combined method to get **Z**;
(3) Per Eq. (25), transform generalized displacements **u** to the basis generalized displacements $\mathbf{u}_b$;
(4) Input the basis generalized displacements $\mathbf{u}_b$ into POD/ROMs based on the basis modeshapes to obtain the generalized aerodynamic force coefficients $\mathbf{f}_b^{ext}$;
(5) Finally, combining reduced fluid model Eq. (32) and the structural dynamic model Eq. (33) to compute the generalized aerodynamic force coefficients corresponding to the modeshapes $\boldsymbol{\Phi}$.

When the global structural parameters are modified, the generalized aerodynamic force corresponding to the modeshapes can be computed quickly by repeating steps 1-5, rather than constructing a new set of POD basis. The approximate method can significantly reduce the computational cost which would be convenient for the transonic aeroelastic stability analysis and optimization with global structural modification.

4 NUMERICAL RESULTS AND DISCUSSION

4.1 POD/ROM solver validation

Before demonstrating the efficiency and accuracy of the proposed ROM interpolation method for transonic aeroelastic problems with global structural parameter variations, the POD/ROM solver is validated firstly using the AGARD 445.6 aeroelastic wing model [49]. The AGARD 445.6 aeroelastic model is with a 45 deg quarter-chord sweep angle, a panel aspect ratio of 1.6525, and a taper ratio of 0.6576 with a symmetrical NACA65A004 airfoil section. The wing material properties were with the density of 381.98 Kg/m^3. The elastic modulus in the span-wise direction and the chord-wise direction is 3.151 and 0.416 GPa, respectively. The shear modulus is 0.4392 GPa. The Poissons ratio of 0.31 [50]. The structural model, shown in Fig. 3(a), consists of 231 nodes and 200 elements. The thickness distribution of the wing was governed by airfoil shape.

A multi-block structured mesh was employed for the flow solver, consisting of 61 computational nodes around each airfoil section and 20 nodes along the wing semispan, as shown in Fig. 3(b). The spatial convergence of the CFD mesh was analyzed in Zhou [20], which reported a good agreement of the results from both the medium and fine grids. The total number of grid points on the medium grid, herein used, is 223,146 ($99 \times 49 \times 46$). Fig. 4 shows the flutter speed predictions computed by the present coupled CFD/CSD solver and the proposed POD/ROM solver. For comparison, experimental data from [49] are also included. The agreement between the ROM and the large computational aeroelastic solver is good for all Mach numbers considered (0.499 to 1.141), including the well-known transonic dip of the flutter speed. The accuracy of both methods have been evaluated over the years in a number of aeroelastic studies [16, 20, 38].

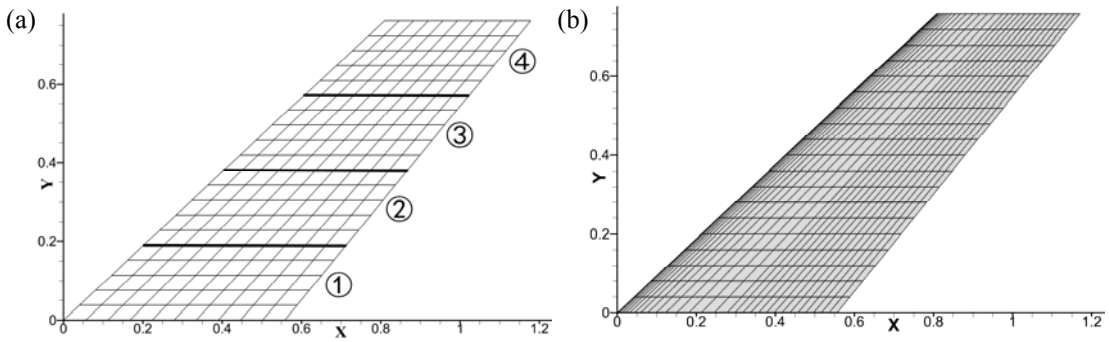

Figure 3: AGARD 445.6 wing: (a) structural model, and (b) surface CFD mesh

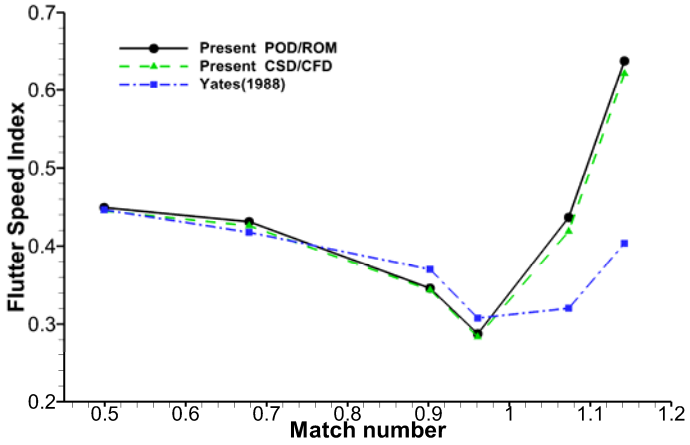

Figure 4: AGARD 445.6 wing flutter boundary; experimental data from [49]

4.2 Accuracy evaluation of the structural dynamic reanalysis model

For exemplification, the structural model of the AGARD 445.6 wing is divided into four spanwise sections, as shown in Fig. 3(a). Each section consists of 50 structural elements of identical material properties, but material properties are allowed to vary from one section to the other. To obtain global variations of the mass and stiffness distribution, material properties are assumed to vary as

$$\text{Section 1, } E_1 = (1+3\varepsilon)E_0, \qquad \rho_1 = (1+3\varepsilon)\rho_0$$

$$\text{Section 2, } E_2 = (1+2\varepsilon)E_0, \qquad \rho_2 = (1+2\varepsilon)\rho_0$$

$$\text{Section 3, } E_3 = (1+\varepsilon)E_0, \qquad \rho_3 = (1+\varepsilon)\rho_0$$

$$\text{Section 4, } E_4 = E_0, \qquad \rho_4 = \rho_0$$

where E_0 and ρ_0 are the Young's modulus and density, respectively, of baseline structural model. It is worth observing that the choice above is used for demonstration purposes and shall not be taken here as a limiting case of the present method. On the contrary, material properties may be thought to vary independently on every single structural element, as commonly practiced in an aeroelastic tailoring study. To assess the accuracy of the ROM in analyzing the modal characteristics of the modified structural model, two criteria are introduced. The first represents the error of the modal frequencies:

$$Error = \frac{f_A^i - f_E^i}{f_E^i} \tag{34}$$

where f_E^i denotes the exact modal frequencies, which are computed through a direct modal analysis, and f_A^i denotes the approximate modal frequencies obtain by the Extended Kirsch combined method. The second criterion is the Modal Assurance Criterion (MAC), defined as:

$$\text{MAC}(\boldsymbol{\Phi}_A, \boldsymbol{\Phi}_E) = \frac{\left|\boldsymbol{\Phi}_E^T \boldsymbol{\Phi}_A\right|^2}{(\boldsymbol{\Phi}_A^T \boldsymbol{\Phi}_A)(\boldsymbol{\Phi}_E^T \boldsymbol{\Phi}_E)} \tag{35}$$

where $\boldsymbol{\Phi}_E$ represents the exact modeshapes (direct modal analysis), and $\boldsymbol{\Phi}_A$ represents the approximate modeshapes (Extended Kirsch combined method). For a perfect match between the exact and approximate modeshape, the MAC is 1.

In the following, three modified cases are considered: $\varepsilon = 1/12,\ 1/6,\ 1/3$. **Fig. 5** shows the modeshapes and associated frequencies for the original and modified AGARD 445.6 wing.

For conciseness, only the case with the largest structural modifications ($\varepsilon = 1/3$) is reported. The first four modeshapes are identified as the first bending, first torsion, second bending, and second torsion, respectively. Quantitatively, the errors between approximate and exact parameters are summarized in **Table 1** for the three values of the modification parameter. For all cases, the error of the modal frequencies is well below one percent. For the MAC, values near unity indicate a good to excellent agreement between the modeshapes of the approximate and exact solutions. The comparison conveys the good predictive capability of the Extended Kirsch combined method to provide approximate modeshapes and frequencies, which are accurate for fast engineering applications, without resorting to a direct modal analysis for each modified structural case.

Parameter	Mode	Exact /Hz	Approximate /Hz	Error/%	MAC
$\varepsilon = 1/12$	1	10.208	10.207	-0.005	1.0000
	2	41.228	41.232	0.010	0.9999
	3	50.756	50.792	0.071	0.9998
	4	95.962	96.034	0.076	0.9991
$\varepsilon = 1/6$	1	10.854	10.856	0.021	1.0000
	2	42.457	42.470	0.030	0.9998
	3	51.819	51.930	0.220	0.9993
	4	96.633	96.873	0.248	0.9970
$\varepsilon = 1/3$	1	11.933	11.943	0.082	0.9999
	2	44.354	44.398	0.101	0.9994
	3	53.591	53.894	0.565	0.9991
	4	97.712	98.412	0.716	0.9911

Table 1: Error of modal frequencies and MAC for the first four modes.

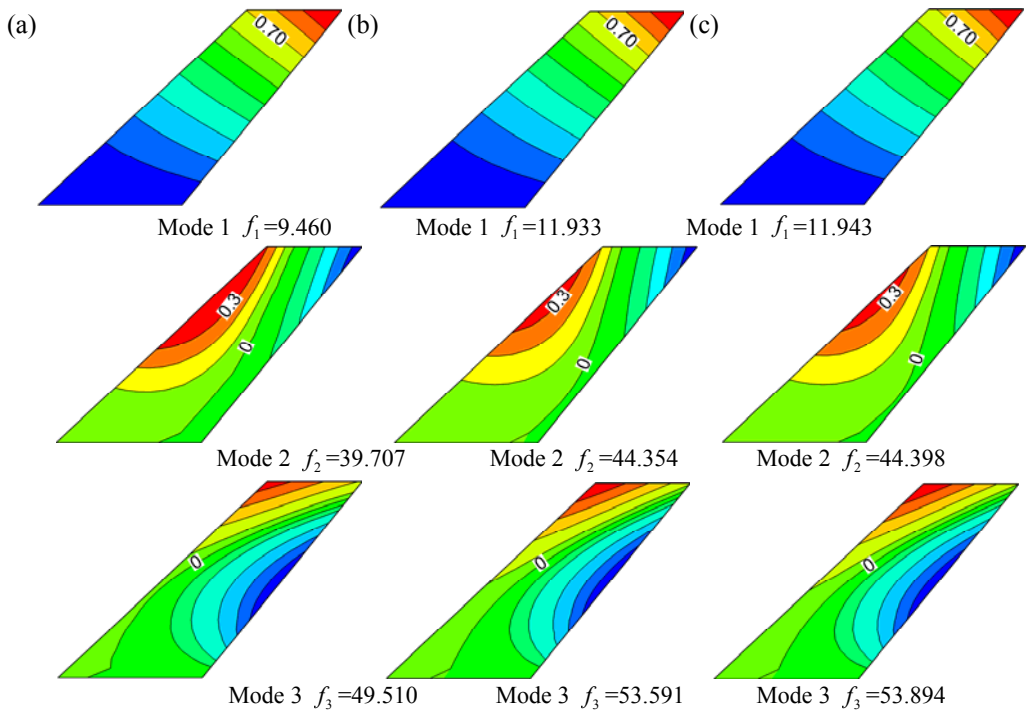

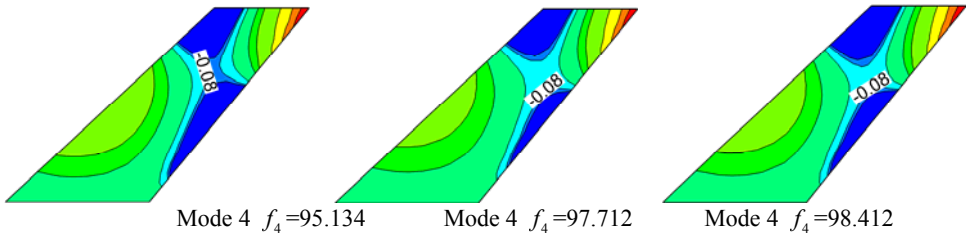

Figure 5: First four modeshapes of the AGARD 445.6 wing: (a) modeshapes and frequencies of original structure, (b) exact modeshapes and frequencies for large modification ($\varepsilon = 1/3$), (c) approximate modeshapes and frequencies for large modification ($\varepsilon = 1/3$).

4.3 Accuracy Evaluation of the POD/ROM interpolation model

After evaluation the accuracy of the POD/ROM model and the structural dynamic reanalysis model of the AGARD 445.6 wing, which are both the key procedures of the proposed new ROM interpolation method, the whole interpolation appropriate POD/ROM will be evaluated in this section. According to the Eq. (32), the approximate POD/ROM method transform the generalized aerodynamic force based on the original modeshapes (as shown in **Fig. 5**(a)) to the aerodynamic responses corresponding to modified modeshapes.

The time histories of the generalized aerodynamic force predicted by the direct POD/ROM and the proposed interpolation appropriate POD/ROM are shown in **Fig. 6**. It should be noted that the direct POD/ROM method has to reconstruct a new set of POD/ROMs to keep the accuracy. For simplifying the description, only the aeroelastic responses with the largest structural parameter modification ($\varepsilon = 1/3$) at the Mach number of 0.960 and the zero angle of (AOA) attack were shown in **Fig.6**. As it can be seen, the aeroelastic responses predicted by both methods agree fairly well. The other cases with the different structural parameter variations have the similar conclusions. The well agreements initially indicate that the proposed interpolation approximate POD/ROM model can accurately capture the generalized unsteady aerodynamic responses corresponding to the global structural parameter variations, even for very large structrual modification such as $\varepsilon = 1/3$.

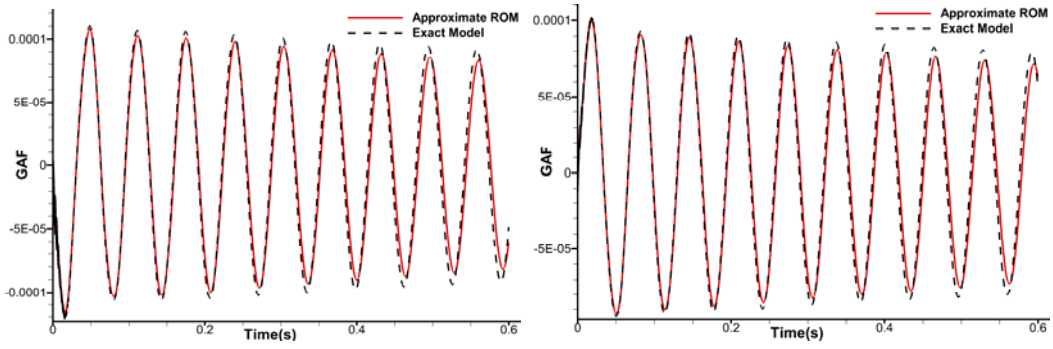

(a) Generalized force of first bending mode (b) Generalized force of first torsion mode

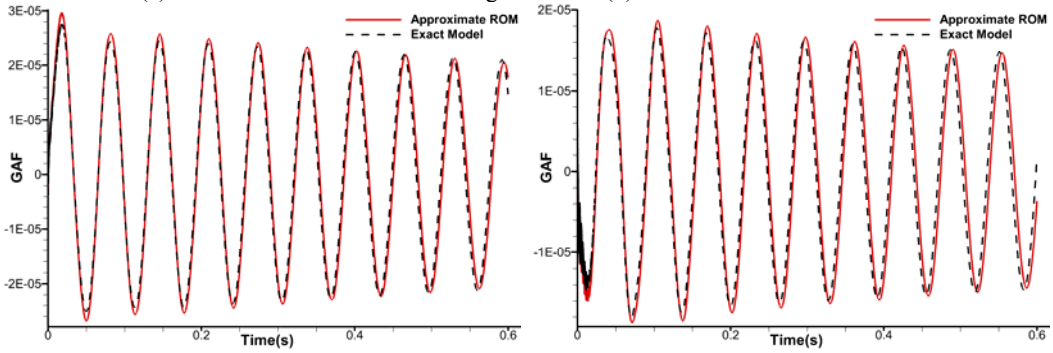

(c) Generalized force of second bending mode (d) Generalized force of second torsion mode

Figure 6 :Comparison of time histories of generalized aerodynamic forces obtain by the direct and approximate method for the largest modification ($\varepsilon = 1/3$).

For further demonstrating the effectiveness and accuracy of the proposed method, two typical aeroelastic structural time responses (decaying and diverging) for the three different structural parameter variation cases under different free stream dynamic pressures are compared as shown in **Fig. 7.** The aeroelastic responses are both obtained by the direct and approximate POD/ROM construction method, respectively. It can be seen that in all the three different structural modification cases, both the divergent and convergent aeroelastic time responses are well consistent. It indicates again that the approximate interpolation POD/ROM method has good accuracy for aeroelastic response prediction of the AGARD 445.6 wing in a very large range of structural parameter variation without reconstructing new POD basis corresponding to the new structural model.

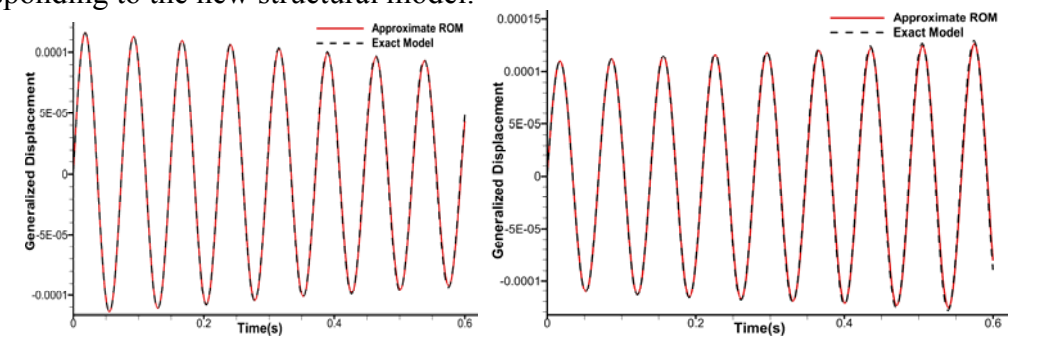

(a) Generalized displacements of first bending mode

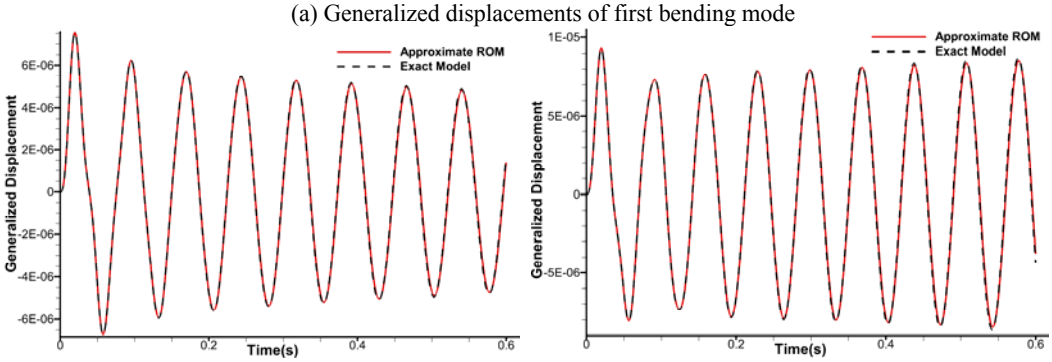

(b) Generalized displacements of first torsion mode

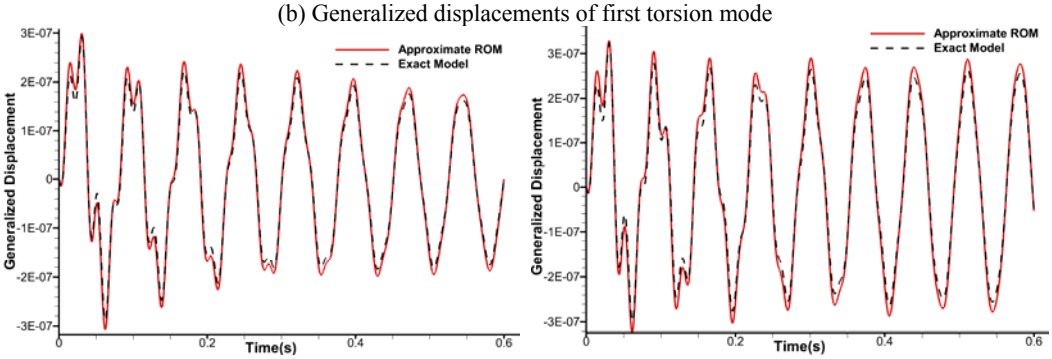

(c) Generalized displacements of second bending mode

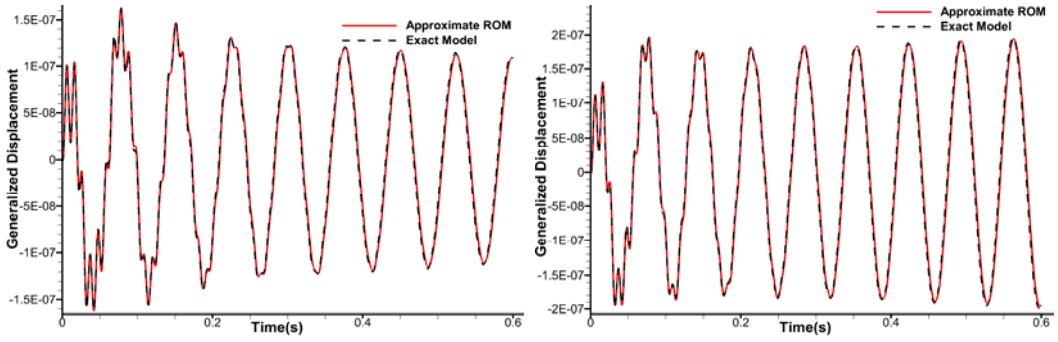

(d) Generalized displacements of second torsion mode

Figure 7:Comparison of time histories of generalized displacements obtain by the direct and approximate method for $\varepsilon = 1/12$ at various dynamic pressures: $V_\infty = 290$ m/s (left), $V_\infty = 320$ m/s (right) (Ma=0.960, AOA=0 deg)

Fig. 9 shows the relationship curve between the system eigenvalue with the largest real part (max(Re(λ))) and speed for the three different degrees of structural variations ($\varepsilon = 1/12,\ 1/6,\ 1/3$), which are predicted by the direct POD/ROM and interpolation appropriated POD/ROM. As shown in **Fig. 10**, the eigenvalue curves predicted by the two POD/ROMs agreed very well in the all three cases.

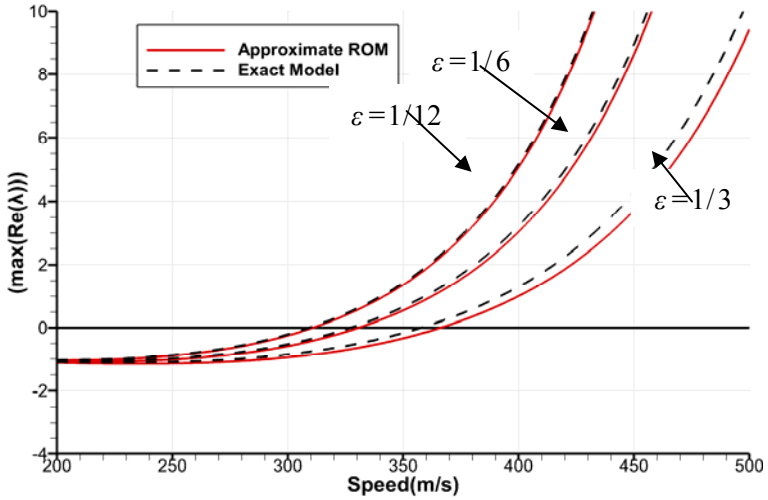

Figure: 9 Relationship curve between the system eigenvalue with the largest real part and Speed for $\varepsilon = 1/12,\ 1/6,\ 1/3$.

The flutter speeds for different structural models predicted by the two POD/ROM methods are also illustrated in **Table 2**. The results show that the flutter speed predicted by the different ROMs are well consistent with each other. Although the deviation of the two methods gradually increased with the increase of the structural parameter changes, the max difference is still littler than 2.21% in the largest modification case. All of the above comparison results indicate that the approximate interpolation POD/ROM method can capture the generalized displacement responses and predict the flutter boundary speed with good accuracy corresponding to the great global structural parameter variation, even for the very large modification ($\varepsilon = 1/3$).

Parameter	Flutter speed (m/s)		
	Driect method	Approximate method	Error (%)
$\varepsilon = 1/12$	309.2	310.8	0.518
$\varepsilon = 1/6$	327.2	330.7	1.070
$\varepsilon = 1/3$	357.7	365.6	2.210

Table 2: Flutter speed obtained by direct and approximate method at Ma=0.960.

4.4 Efficiency Evaluation of the POD/ROM interpolation model

Our objective is to propose an new efficient automatically interpolation POD/ROM model which is suitable for the routine aeroelastic design optimization and test operations. So that the computational efficiency is much more important performance of the interpolation POD/ROM method for the multidisciplinary design optimization and uncertainty analysis. All of these simulations are performed on a Windows 7 system PC with Intel® Core(TM) i7-2600 CPU (3.40 GHz, 8 cores, but only one core used) and 16 GB RAM. The computational cost of the direct and approximate interpolation POD/ROM method is listed in **Table 3**. For the three structural modification cases, the direct POD/method have to reconstruct the new POD/ROM for three times. However, without the most expensive time-consuming reconstruction procedure (one time 16 hours for AGARD 445.6 wing), the computational cost of the interpolation approximate POD/ROMM method is reduced obviously, especially at least three-order times compared after the POD/ROM was constructed (e.g., 48h5.25s/18.39s＝9411.8).

Suppose the application of the direct and approximate POD/ROM method in the aeroelastic flutter design optimization where the structure parameters would change 1000 times, and 20 free stream dynamic pressure values were input for searching the flutter point and the aeroelastic responses at each fixed AGARD 445.6 structural model. The computational cost for the direct POD/ROM method would be $16h\times1000+1.75s\times20\times1000=16009.72$ hours which is about 667 days. However the computational cost of the interpolation approximate POD/ROM method is only $16h\times1+0.76s\times1000+1.75s\times20\times1000=26.16h$ about which is only little more than one day. The demonstration case indicated that the proposed interpolation POD/ROM method is very computational efficiency with at least for two orders of magnitude time reduction than the traditional direct POD/ROM reconstruction method, which is very suitable for aeroelastic optimization and uncertainty analysis with large global structural parameter variation.

Method	Process	CPU time
Direct	Construct a new set of POD/ROMs	16*h*
	Time histories responses of the generalized displacement for a values of free stream dynamic pressure	1.75s
	Three structural parameter variation ($\varepsilon = 1/12$,1/6,1/3)	48*h* 5.25*s*
	Structure optimization with 1000 structural parameter change	16097.22*h*
Approximate	Construct the initial set of POD/ROMs for original structure	16*h*
	Compute **Q** use Extended Kirsch combined method	0.76*s*
	Time histories responses of the generalized displacement for a values of free stream dynamic pressure based	1.79*s*
	Three structural parameter variation ($\varepsilon = 1/12$,1/6,1/3)	16*h* 18.39*s*
	Structure optimization with 1000 structural parameter change	26.16*h*

Table 3: Computational cost of the direct and approximate POD/ROM method.

5 CONCLUSIONS

The feasibility and the accuracy of the approximate interpolation POD/ROM method was demonstrated and evaluated by the AGARD 445.6 aeroelastic wing model with a large range of global structural parameter changes. The accuracy and efficiency of the key procedures were evaluated and compared firstly with the direct numerical simulation, including the original basic POD/ROM and the extended Kirsch combined structural reanalysis method. And then the accuracy of the proposed interpolation POD/ROMs were evaluated for the different aeroelastic time responses compared with the direct POD/ROMs, including the general unsteady aerodynamic coefficients and the general modal displacements with three different structural parameter modification cases in different free steam velocities. The stability eigenvalue curve and the flutter points were also compared for different modified aeroelastic models in transonic flows. The good agreements of the numerical results show that the proposed approximate POD/ROM interpolation method can capture the transoinc aeroelastic characteristics of the aeroelastic system with large range global structural parameter variations with good accuracy. The deviation of the interpolation POD/ROM will slight slowly grows with the increase of structural parameter variation, however it could keep the enough accuracy in a large range of structural parameter variation which can be determined previously when the structural stiffness and mass change.

The most advantage of the proposed interpolation POD/ROM is not only keeping the accuracy corresponding to the aerelastic system's structural parameter variation, but also is the great reduction of the computational cost. Without the most expensive time-consuming new POD basis reconstruction procedure required in the traditional direct POD/ROM method, the efficiency of the proposed appropriate POD/ROMs can be improved at least two-order magnitude according to the demonstration case. The proposed automatic efficient interpolation procedure provides a potential powerful tool for the CFD-based POD/ROM's application in the transonic aeroelastic optimization and uncertainty analysis where the global structural parameter variation is ordinary. In the future work, we will apply the proposed method to the aeroelastic flutter optimization and also investigate the aeroelastic uncertainty analysis based on the CFD-based ROMs, which are very challenge topics in transonic nonlinear aeroelasticity.

REFERENCES AND CITATIONS

[1] G.P. Guruswamy, Unsteady aerodynamic and aeroelastic calculations for wings using Euler equations, AIAA journal, 28 (1990) 461-469.

[2] J. Sahu, F. Fresconi, K. Heavey, Unsteady Aerodynamic Simulations of a Finned Projectile at a Supersonic Speed with Jet Interaction, 32nd AIAA Applied Aerodynamics Conference, 2014, pp. 3024.

[3] D.M. Schuster, D.D. Liu, L.J. Huttsell, Computational aeroelasticity: success, progress, challenge, Journal of Aircraft, 40 (2003) 843-856.

[4] R. Yurkovich, Status of unsteady aerodynamic prediction for flutter of high-performance aircraft, Journal of Aircraft, 40 (2003) 832-842.

[5] E.H. Dowell, J.P. Thomas, K.C. Hall, Transonic limit cycle oscillation analysis using reduced order aerodynamic models, Journal of Fluids and Structures, 19 (2004) 17-27.

[6] D.J. Lucia, P.S. Beran, P.I. King, Reduced-order modeling of an elastic panel in transonic flow, Journal of Aircraft, 40 (2003) 338-347.

[7] D.E. Raveh, Gust-response analysis of free elastic aircraft in the transonic flight regime, Journal of Aircraft, 48 (2011) 1204-1211.

[8] [8] P.G. A. Cizmas, A. Palacios, Proper orthogonal decomposition of turbine rotor-stator interaction, Journal of propulsion and power, 19 (2003) 268-281.

[9] S.T. Clark, R.E. Kielb, K.C. Hall, Developing a Reduced-Order Model to Understand Non-Synchronous Vibration (NSV) in Turbomachinery, ASME Turbo Expo 2012: Turbine Technical Conference and Exposition, 2012, pp. 1373-1382.

[10] S. Mariappan, A.D. Gardner, R. Kai, M. Raffel, Analysis of Dynamic Stall Using Dynamic Mode Decomposition Technique, Aiaa Journal, 52 (2014) 2427-2439.

[11] B. Stanford, P. Beran, Cost reduction techniques for the structural design of nonlinear flapping wings, 50th AIAA/ASME/ASCE/AHS/ASC Structures, Structural Dynamics, and Materials Conference 17th AIAA/ASME/AHS Adaptive Structures Conference 11th AIAA No, 2009, pp. 2414.

[12] L. Demasi, A. Palacios, A reduced order nonlinear aeroelastic analysis of joined wings based on the proper orthogonal decomposition, 51st AIAA/ASME/ASCE/AHS/ASC Structures, Structural Dynamics, and Materials Conference 18th AIAA/ASME/AHS Adaptive Structures Conference 12th, 2010, pp. 2722.

[13] H. Hesse, R. Palacios, Reduced-order aeroelastic models for dynamics of maneuvering flexible aircraft, AIAA journal, 52 (2014) 1717-1732.

[14] T. Lieu, C. Farhat, M. Lesoinne, Reduced-order fluid/structure modeling of a complete aircraft configuration, Computer methods in applied mechanics and engineering, 195 (2006) 5730-5742.

[15] D. Amsallem, C. Farhat, T. Lieu, Aeroelastic analysis of F-16 and F-18/A configurations using adapted CFD-based reduced-order models, 48th AIAA/ASME/ASCE/AHS/ASC Structures, Structural Dynamics, and Materials Conference, 2007, pp. 2364.

[16] Q. Zhou, G. Chen, Y. Li, a Reduced Order Model Based on Block Arnoldi Method for Aeroelastic System, International Journal of Applied Mechanics, 6 (2014) 1450069.

[17] G. Chen, X. Wang, Y. Li, REDUCED-ORDER-MODEL-BASED PLACEMENT OPTIMIZATION OF MULTIPLE CONTROL SURFACES FOR ACTIVE AEROELASTIC CONTROL, International Journal of Computational Methods, 11 (2014) 1350081.

[18] G. Chen, J. Sun, W. Mao, Y. Li, Limit Cycle Oscillation Control for Transonic Aeroelastic Systems Based on Support Vector Machine Reduced Order Model, Transactions of the Japan Society for Aeronautical and Space Sciences, 56 (2013) 8-14.

[19] Q. Zhou, C. Gang, L. Yueming, D.R. Andrea, Aeroelastic Moving Gust Responses and Alleviation based on CFD, AIAA Modeling and Simulation Technologies Conference, 2016, pp. 3837.

[20] Q. Zhou, D.-f. Li, A. Da Ronch, G. Chen, Y.-m. Li, Computational fluid dynamics-based transonic flutter suppression with control delay, Journal of Fluids and Structures, 66 (2016) 183-206.

[21] B.I. Epureanu, E.H. Dowell, K.C. Hall, Mach number influence on reduced-order models of inviscid potential flows in turbomachinery, Journal of fluids engineering, 124 (2002) 977-987.

[22] T. Lieu, C. Farhat, Adaptation of POD-based aeroelastic ROMs for varying mach number and angle of attack: application to a complete F-16 configuration, AIAA paper, 7666 (2005) 2005.

[23] T. Lieu, C. Farhat, Adaptation of aeroelastic reduced-order models and application to an F-16 configuration, AIAA journal, 45 (2007) 1244-1257.

[24] T. Lieu, M. Lesoinne, Parameter adaptation of reduced order models for three-dimensional flutter analysis, AIAA Paper, 888 (2004) 2004.

[25] G. Chen, Y. Li, G. Yan, A nonlinear POD reduced order model for limit cycle oscillation prediction, Science China Physics, Mechanics and Astronomy, 53 (2010) 1325-1332.

[26] G. Chen, Y. Zuo, J. Sun, Y. Li, Support-vector-machine-based reduced-order model for limit cycle oscillation prediction of nonlinear aeroelastic system, Mathematical problems in engineering, 2012 (2012).

[27] C. Gang, S. Jian, L. Yueming, Active flutter suppression control law design method based on balanced proper orthogonal decomposition reduced order model, Nonlinear Dynamics, 70 (2012) 1-12.

[28] R. Hayes, W. Yao, S.P. Marques, The Influence of Structural Variability on Limit Cycle Oscillation Behaviour, Aiaa/issmo Multidisciplinary Analysis and Optimization Conference, 2014, pp. 63.

[29] C.L. Fenwick, D.P. Jones, A.L. Gaitonde, Consideration of ROM interpolation for aeroelastic design using structural modification, DOI (2007).

[30] W. Zhang, K. Chen, Z. Ye, Unsteady aerodynamic reduced-order modeling of an aeroelastic wing using arbitrary mode shapes, Journal of Fluids & Structures, 58 (2015) 254-270.

[31] P. Gasbarri, L.D. Chiwiacowsky, H.F.D.C. Velho, A hybrid multilevel approach for aeroelastic optimization of composite wing-box, Structural & Multidisciplinary Optimization, 39 (2010) 607-624.

[32] P.D. Ciampa, B. Nagel, M.V. Tooren, Global Local Structural Optimization of Transportation Aircraft Wings, Aiaa Structures, Structural Dynamics, and Materials Conference, 2010.

[33] B. Van Leer, Towards the ultimate conservative difference scheme. V. A second-order sequel to Godunov's method, Journal of computational Physics, 32 (1979) 101-136.

[34] T. PULLIAM, Time accuracy and the use of implicit methods, 11th Computational Fluid Dynamics Conference, 1993, pp. 3360.

[35] R. Chen, Z. Wang, Fast, block lower-upper symmetric Gauss-Seidel scheme for arbitrary grids, AIAA journal, 38 (2000) 2238-2245.

[36] R.L. Harder, R.N. Desmarais, Interpolation using surface splines, Journal of aircraft, 9 (1972) 189-191.

[37] H. Tsai, A. F. Wong, J. Cai, Y. Zhu, F. Liu, Unsteady flow calculations with a parallel multiblock moving mesh algorithm, AIAA journal, 39 (2001) 1021-1029.

[38] G. Chen, J. Sun, Y.-M. Li, Adaptive reduced-order-model-based control-law design for active flutter suppression, Journal of Aircraft, 49 (2012) 973-980.

[39] K.C. Hall, J.P. Thomas, E.H. Dowell, Proper orthogonal decomposition technique for transonic unsteady aerodynamic flows, AIAA journal, 38 (2000) 1853-1862.

[40] T. Lieu, C. Farhat, M. Lesoinne, POD-based aeroelastic analysis of a complete F-16 configuration: ROM adaptation and demonstration, 46th AIAA/ASME/ASCE/AHS/ASC Structures, Structural Dynamics and Materials Conference, 2005, pp. 2295.

[41] T. Lieu, M. Lesoinne, Parameter adaptation of reduced order models for three-dimensional flutter analysis, 42nd AIAA Aerospace Sciences Meeting and Exhibit, 2004, pp. 888.

[42] Q. Song, P. Chen, S. Sun, An exact reanalysis algorithm for local non-topological high-rank structural modifications in finite element analysis, Computers & Structures, 143 (2014) 60–72.

[43] M.A. Akgün, J.H. Garcelon, R.T. Haftka, Fast exact linear and non‐linear structural reanalysis and the Sherman‐Morrison–Woodbury formulas, International Journal for Numerical Methods in Engineering, 50 (2001) 1587-1606.

[44] J.-G. Beliveau, S. Cogan, G. Lallement, F. Ayer, Iterative least-squares calculation for modal eigenvector sensitivity, AIAA journal, 34 (1996) 385-391.

[45] S.H. Chen, X.W. Yang, Extended Kirsch combined method for eigenvalue reanalysis, AIAA journal, 38 (2000) 927-930.

[46] U. Kirsch, M. Bogomolni, I. Sheinman, Efficient Dynamic Reanalysis of Structures, Journal of Structural Engineering, 133 (2007) 440-448.

[47] S. Chen, X. Yang, H. Lian, Comparison of several eigenvalue reanalysis methods for modified structures, Structural and Multidisciplinary Optimization, 20 (2000) 253-259.

[48] S.H. Chen, D.T. Song, A.J. Ma, Eigensolution reanalysis of modified structures using perturbations and Rayleigh quotients, Communications in numerical methods in engineering, 10 (1994) 111-119.

[49] E.C. Yates, AGARD standard aeroelastic configuration for dynamic response, candidate configuration I, Wing, 445 (1987) 103-129.

[50] J. Zhong, Z. Xu, Coupled fluid structure analysis for wing 445.6 flutter using a fast dynamic mesh technology, International Journal of Computational Fluid Dynamics, 30 (2016) 531-542.

COPYRIGHT STATEMENT